Cellulose (2022) 29:7263–7276
https://doi.org/10.1007/s10570-022-04721-4

ORIGINAL RESEARCH

Double-emulsion templated macroporous cellulose microspheres as a high-performance chromatographic media for protein separation

Liangzhi Qiao · Yuxin Liao · Xiawen Wang · Shanshan Wang · Kaifeng Du

Received: 21 January 2022 / Accepted: 13 June 2022 / Published online: 5 July 2022

Abstract Cellulose microspheres are commonly chromatographic media yet seriously limited in biomacromolecules separation and purification due to the slow mass transfer kinetics resulting from their narrow nanopores. Herein, a macroporous cellulose microsphere (MCM) with enhanced mass transfer ability has been successfully developed by an oil-in-water-in-oil ($O_1/W/O_2$) double emulsion strategy. The evolution profile of the double emulsion was tracked and achieved the optimization of interconnected macroporous structure. The macroporous structure not only provide fast mass transfer pathways for proteins but also increase the accessibility of meso/micropores. Benefitting from the macropores, the obtained diethylaminoethyl-modified MCM (DEAE-MCM) exhibits high permeability (3.81×10^{-13} m^2), and fast adsorption rate (reaching equilibrium within 40 min) and high adsorption capacity (334.21 mg/g) for bovine serum albumin, far superior to commercially DEAE Sepharose Fast Flow. More importantly, under the high flow rate, DEAE-MCM remains a high dynamic adsorption capacity, promising it for fast protein chromatography.

Keywords Cellulose microsphere · Protein · Adsorption · Chromatography · Macropores

Introduction

With the rapid development of bioindustry, more and more bioproducts with large molecule size such as proteins need to be separated (Farid et al. 2020; Love et al. 2013; Smith 2005). As such, there is an urgent demand to develop highly efficient separation processes to produce high-quality bioproducts (Smith 2005). To meet the quality requirements, downstream separation costs can account for more than 60% of the total cost of biomanufacturing process (Shukla et al. 2007). As the most important process in downstream separation processing, liquid chromatography (LC) has been commonly used for the separation and purification of biomacromolecules because of its mild process and high resolution. In this context, considerable attention has been paid to the design and development of high-performance LC to satisfy the large and rigorous requirements of biomacromolecule separation and purification.

In terms of the separation efficiency of LC, it mainly depends on the properties of chromatographic media that is the heart of LC technology, which usually consists of porous media like microspheres

Supplementary Information The online version contains supplementary material available at https://doi.org/10.1007/s10570-022-04721-4.

L. Qiao · Y. Liao · X. Wang · S. Wang · K. Du (✉)
Department of Pharmaceutical and Biological Engineering, School of Chemical Engineering, Sichuan University, No.24 South Section 1, Yihuan Road, Chengdu 610065, People's Republic of China
e-mail: kfdu@scu.edu.cn

modified with specific ligands to capture the target biomacromolecules by one or more certain interactions, such as ion-exchange, affinity, and hydrophobic interaction (Schlitz 1984; Zhang et al. 2014). Several chromatographic media including polysaccharides (Li et al. 2015; Oshima et al. 2011, 2014), inorganic compounds (Beyki et al. 2017; Qiao et al. 2019), and polymers (Song et al. 2019; Zhang et al. 2014), have been widely used. Among them, polysaccharide microspheres, such as cellulose, agarose, and glucan microspheres, have received significant attention as a base support for chromatography media due to their ability to minimize the nonspecific adsorption (Fu et al. 2016; Gericke et al. 2013). Moreover, these polysaccharides have abundant hydroxyl groups, which could be easily modified to graft specific ligands by various functional methods (Feng et al. 2020; Roy et al. 2009). However, the application of polysaccharide microspheres as chromatography media are limited due to their narrow nanopores (< 100 nm). The narrow nanopores not only cause a slow mass transfer kinetic for biomacromolecules (Gustavsson and Larsson 1999; Wang et al. 2007), but also lead to the inaccessibility of a number of binding sites in the internal pores due to the long diffusion path and large flow resistance.

Enlarging pore size is one of the most effective ways to improve the mass transfer of chromatography media (Zhao et al. 2019), which can achieve a fast separation rate with a high adsorption capacity. Macroporous structure not only can provide wide channels through chromatography media for the convective flow of mobile phase for enhancing mass transfer, but also short the path from bulk solution to the interior nanopores, increasing the accessibility of adsorption sites. Unfortunately, there are only a few effective methods reported on the preparation of macroporous media. We previously reported macroporous cellulose beads fabricated by emulsification using solid particles ($CaCO_3$) as porogen (Du et al. 2010). Although a lower equilibrium adsorption capacity for BSA, the macroporous cellulose beads had a higher dynamic adsorption capacity of 47.7 mg/mL compared with commercially available DEAE Sepharose Fast Flow (DEAE-FF), demonstrating the improvement of the macropores on the chromatography performance. However, the solid-template method was difficult to form interconnected pore structure unless a high content of solid template was used, which would in turn cause poor mechanical strength due to the formation of overmuch pores. Moreover, the removal of solid templates required harsh conditions, which made the fabrication process more complicated and unsustainable. Moreover, double emulsion strategy has been widely reported to fabricate macroporous polysaccharide microspheres. The macroporous structure was created by the coalescence between interior O_1 droplets and external O_2 continuous phase. However, although extensive literatures existed, the preparations of double emulsion were often determined empirically and the obtained pore structure therefore varied from case to case. Thus, facile and effective methods for creating macroporous structure in polysaccharide microspheres are highly desired.

In this study, we adopted a facile double emulsion strategy for fabricating macroporous cellulose microspheres (MCM) to improve their mass transfer ability. The evolution profile of the double emulsion was tracked and achieved the optimization of macroporous structure. The macroporous structure was expected to provide fast mass transfer pathways and increase the accessibility of meso/micropores. Further, the obtained MCM was modified with diethylaminoethyl chloride (DEAE-HCl) to obtain an ion-exchange adsorbent (DEAE-MCM). The permeability, specific surface area, and pore size distribution of DEAE-MCM were carefully characterized and compared with those of commercially DEAE-FF. The adsorption kinetic and adsorption isotherm of DEAE-MCM were further investigated to elucidate the effect of macropores on the adsorption performances.

Experimental section

Materials

Cellulose in particle form (particle size: 90–150 μm) was provided from Macklin Biochemical Technology Co., Ltd. (Shanghai, China). Diethylaminoethyl chloride (DEAE-HCl) and bovine serum albumin (BSA) were obtained from Aladdin Reagent Co., Ltd. (Shanghai, China). DEAE Sepharose Fast Flow (DEAE-FF) was purchased from GE healthare (USA). Other reagents, such as NaOH, thiourea, Tween-80, Span-80, sulfuric acid, ethanol, glycol

diglycidyl ether, and epichlorohydrin, were purchased from Kelong Chemical (Chengdu, China).

Preparation of MCM

Firstly, 3 g of cellulose was dissolved in 50 mL of NaOH (12 wt%)/thiourea (8 wt%) aqueous solution in an ice bath to obtain a transparent cellulose solution. 800 µL of glycol diglycidyl ether was dropped into the cellulose solution to improve the mechanical strength of MCM by chemical cross-linking. Next, 10 mL of hexane (O_1) and 0.1 g of Tween-80 were poured into 20 mL of cellulose solution (W) at 800 rpm for 5 h to form the O_1/W emulsion. Then, the O_1/W emulsion was further poured into 120 mL of liquid paraffin (O_2) containing 10 g of Tween-80 at 200 rpm to form the O_1/W/O_2 emulsion. After emulsification for 1 h at room temperature, 50 mL of ethanol (50 vt%) aqueous solution was poured into the O_1/W/O_2 emulsion to solidify the cellulose microspheres. The obtained cellulose microspheres were rinsed thoroughly with ethanol and deionized water.

Preparation of DEAE-MCM

MCM was modified by using DEAE-HCl as ligands according to a previously reported method by us (Qiao et al. 2020) (Fig. S1). Briefly, 100 mg of wet MCM was added in 20 mL of 3.0 mol/L DEAE-HCl solution and the mixture was heated to 60 °C for 30 min. Next, 20 mL of 3.0 mol/L NaOH solution was poured into the mixture. After 2 h at 60 °C, the mixture was cooled and the microspheres were washed thoroughly with deionized water. The obtained microspheres were named DEAE-MCM.

Characterization

All samples were dried prior to characterization as follows. 1 g of wet DEAE-MCM was exchanged stepwise with 10 mL of *t*-BuOH solutions (20% increment, from 0 to 100% *t*-BuOH) and then frozen in liquid nitrogen for 5 min followed by freeze-drying for 12 h by a Biocool FD-1A-50 lyophilizer. Fourier-transformed infrared (FT-IR) spectroscopy measurement was conducted on a Spectrum TwoLi10014 Fourier transform infrared spectrometer (FT-IR) in the wavelength of 4000–400 cm^{-1}. The chemical composition and surface chemical states of microspheres were examined with X-ray photoelectron spectrometry (XPS, ESCALAB 250Xi). X-ray diffraction (XRD) patterns were measured by an XRD diffractometer (D8-Advance, Bruker) from 10 to 60° using Cu Ka radiation at a voltage of 40 kV and a current of 30 mA. The microscopic structure of microspheres was observed by JSM 7610F scanning electron microscopy. The ÄKTA Explorer 100 System was used to load the sample into HR 5/10 column to perform the flow hydrodynamic experiment and breakthrough experiments, and the back pressure of the sample column at different flow rates was measured by changing the flow rate of water. N_2 adsorption–desorption isotherms were measured with a Micromeritics ASAP 2020 analyzer. The specific surface area was calculated according to Brunauer–Emmett–Teller (BET) model, and the pore size distribution was calculated according to Barrett–Joyner–Halenda (BJH) method. The porosity of microspheres was calculated using the following Eq. (1):

$$\text{Porosity}\,(\%) = \left(1 - \rho_a/\rho_c\right) \times 100\% \tag{1}$$

where ρ_a and ρ_c are the volumetric mass densities of dry microspheres and solid scaffold of cellulose, respectively. ρ_c was fixed at 1500 kg/m^3 according to literature data (Sehaqui et al. 2010).

The swelling ratios of the microspheres were measured by soaking the microspheres in different buffer solutions (Tris–HCl buffer with different NaCl concentration (0, 20, 50, and 100 mM)). At 24 h, the microspheres were blotted with filter paper to remove surface water until the weight no longer change. The swelling ratio (SR) was determined with the following Eq. (2):

$$\text{SR} = \left(\text{W}_1 - \text{W}_0\right)/\text{W}_0 \times 100\% \tag{2}$$

where W_0 (g) was the mass of microspheres in water, W_1 (g) was the weight of the sample soaked in buffer solution".

The ion exchange capacity of adsorbent has been estimated by silver chloride precipitation titration. Briefly, the microspheres were exchanged with 10 mL of NaCl solution (1 mol/L), 10 mL of HCl solution (0.1 mol/L), and 100 mL of HCl solution (0.0001 mol/L) in turn to ensure the complete exchange of chloride ions. Then, a certain amount (~1.0 g) of the anion exchangers was dehydrated

and added to 20 mL of Na_2SO_4 solution (10%, w/w) followed by incubating at 25 °C for 1 h to replace chloride ions. Finally, the chloride ion concentration of the supernatant was measured by titrating using 0.01 mol/L of $AgNO_3$ solution, and 10% (w/w) of K_2CrO_4 solution was used as the indicator. The ionic capacities of the anion exchangers were calculated by mass balance.

Protein adsorption isotherms

In the batch adsorption, a series of 10 mg adsorbent was added separately into 10 mL of Tris–HCl buffer solution with pH = 7.4. Different BSA concentrations in the ranges of 0–1.2 mg/mL were contained in the buffer solution. The mixtures were gently stirred at room temperature at 100 rpm, and maintained for 80 min to adsorb BSA. After completing the adsorption, the suspension was centrifuged. The BSA concentration of the supernatant was tested with UV/Vis spectrophotometer at 280 nm. Finally, the adsorption amount of adsorbent was calculated by mass balance before and after the experiment according to the Eq. (3). Further, the adsorption data were fitted with the Langmuir model (4).

$$q_e = \frac{\left(c_0 - c_e\right)V}{m} \tag{3}$$

$$q_e = \frac{q_m c_e}{k_d + c_e} \tag{4}$$

where q_e (mg/g) and q_m (mg/g) are the experimental and fitted equilibrium adsorption capacity, respectively; c_0 (mg/mL) and c_e (mg/mL) are the initial and equilibrium BSA concentrations, respectively; V(mL) is the volume of BSA solution, and M (g) is the mass of adsorbent; K_d (mL/mg) is a dissociation constant of Langmuir model.

Protein adsorption kinetics

10 mg of adsorbent was added to 10 mL of BSA solution with an initial concentration of 0.8 mg/mL for BSA. Nine parallel experiments were respectively carried out at various time intervals (3, 5, 10, 15, 20, 25, 30, 50, 90 min). At each defined time interval, BSA concentration was determined. The adsorption kinetic data were fitted with pseudo-first-order (5) and pseudo-second-order model (6), respectively.

$$q_t = q_e\left(1 - e^{-k_1 t}\right) \tag{5}$$

$$q_t = \frac{k_2 q_e^2 t}{1 + k_2 q_e t} \tag{6}$$

where q_e and q_t (mg/g) are adsorption capacity of BSA at equilibrium and at a real time t (min), respectively; k_1 (1/min) and k_2 (mg/g/min) are pseudo-first-order and pseudo-second-order adsorption kinetic parameters, respectively.

Effect of ionic strength

10 mg of adsorbent was added to 10 mL of 0.8 mg/mL of BSA solution with different NaCl concentrations (20, 50, and 100 mM). After completing the adsorption, BSA concentration was determined.

Reusability

The 10 mg of adsorbent was added to 10 mL of BSA solution (8 mg/mL) for adsorption. After adsorption was completed, the saturated adsorbent was eluted by being immersed into 1.0 mol/L of NaCl solution (pH = 7.4) for 3 h for desorption (Bowes and Lenhoff 2011; Yu and Sun 2013), followed by washing with buffer solution (pH = 7.4). The adsorption/desorption cycles were performed five times to study the reusability of adsorbent.

Breakthrough experiment

The dynamic adsorption capacities of adsorbents were conducted with ÄKTA Explorer 100 System). Microspheres were packed into HR 5/10 column. The column was firstly equilibrated with 20 mL of buffer solution, and then 0.8 mg/mL of BSA solution was continuously flowed through the column at a flow rate of 0.5 mL/min. Elute was online analyzed by an integrated UV detector.

Results and discussion

Preparation and characterization of DEAE-MCM

DEAE-MCM was fabricated through a double emulsion strategy followed by modification with DEAE, as shown in Fig. 1. The $O_1/W/O_2$ double emulsion strategy was adopted to create the macroporous structure. During the preparation of the double emulsion, a certain amount of the internal oil phase (O_1) composed of hexane and Tween-80 was first emulsified into cellulose solution (aqueous phase (W)) at a high shear rate, forming an O_1/W simple emulsion. Then, the O_1/W emulsion was further dispersed into an external oil phase (O_2) composed of liquid paraffin and Tween-80 at a lower shear rate and shorter time to form an $O_1/W/O_2$ double emulsion. As a metastable system, the double emulsion has several evolution behaviors, including inter coalescence between O_1 droplets, burst escape of O_1 droplets, and coalescence of O_1 and O_2 phases. Under the given conditions, the interior O_1 droplets prefer to coalesce with the external O_2 continuous phase through the W phase (Fig. 2B). Such a preference would lead to the formation of oil channels. Taking advantage of the coalescence behavior, we can convert oil channels into macropores by solidifying the cellulose aqueous phase. We anticipate that the macropores provide fast mass transfer pathways for proteins, thus improving the separation efficiency.

Previous studies reported that there are two key factors to affect the evolution behavior of double emulsion: the stability of interfaces and the osmotic gradient between O_1 and O_2 (Na et al. 2012). When the internal interfaces (O_1/W) are better stabilized than the external ones (W/O_2), coalescence between O_1 and O_2 would dominate the emulsion evolution (Na et al. 2012). Therefore, we chose Tween-80 as the surfactant of the double emulsion to induce the unstable interface because of its high hydrophilic, and

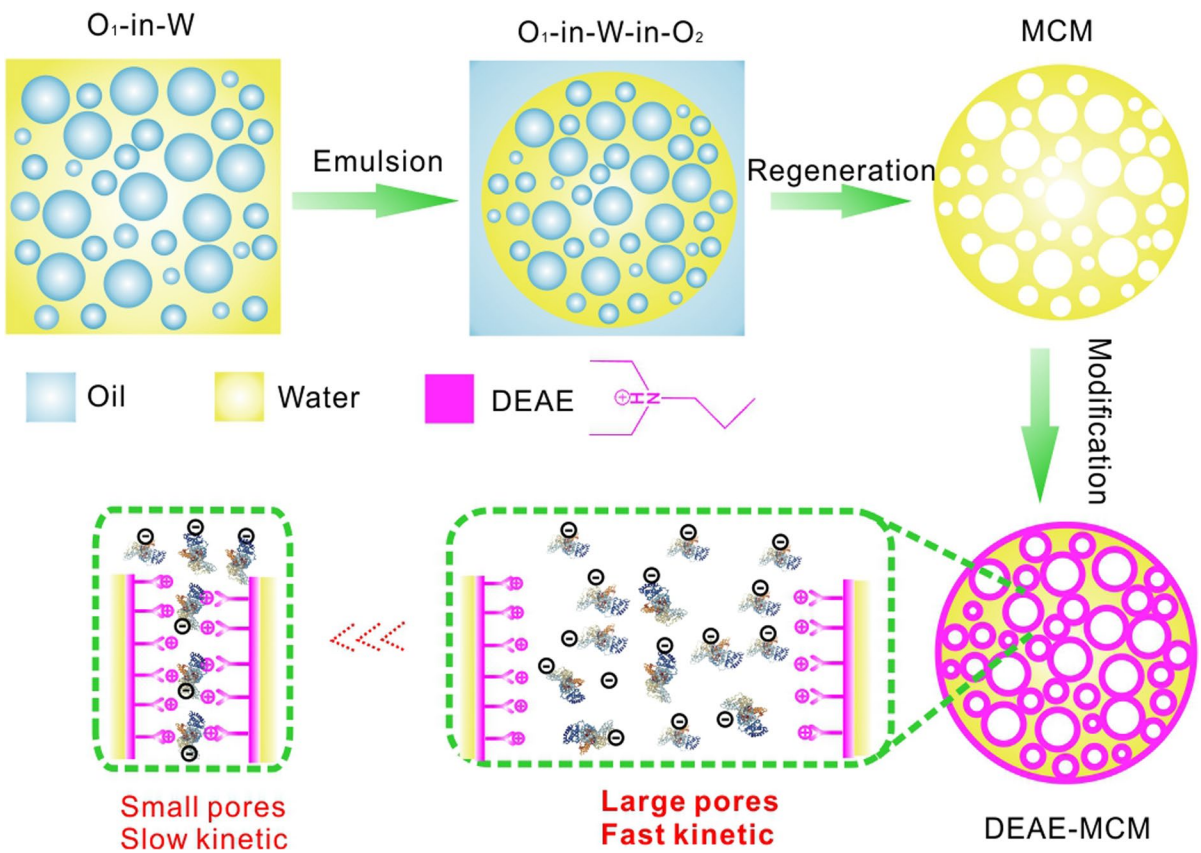

Fig. 1 Schematic illustration of the preparation of DEAE-MCM and its advantage for adsorbing proteins

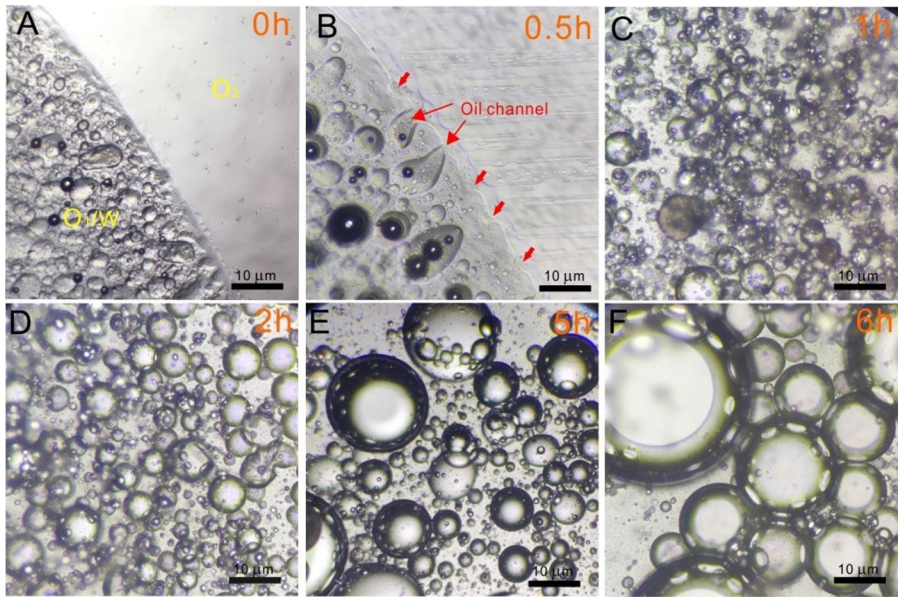

Fig. 2 Optical micrographs of the $O_1/W/O_2$ double emulsion interface at different times: 0 h (**A**), 0.5 h (**B**), 1 h (**C**), 2 h (**D**), 5 h (**E**), and 6 h (**F**)

further in situ monitored the evolutions of the double emulsion and MCM, as shown in Figs. 2 and 3. At the early stage (< 2 h) of the double emulsion, there are a number of small O_1 drops in W phase (Fig. 2A–C). When solidification happens at this stage, MCM shows a homogeneous macroporous structure with an average pore diameter of 1.59 μm (Fig. 3B, S2), the ratio of opening pore area is estimated to be about 18.83% (Fig. S3). After a certain period of ripening (2–5 h), there are fewer and larger O_1 drops in the double (Fig. 2D, E). This is due to that the interior coalescence between O_1 droplets. The phenomenon is similar to previous reports that multiple emulsions tend to collapse to more stable simple O/W or W/O emulsions (Gao et al. 2009). When the solidification is initiated, the obtained MCM shows a fewer and larger pore structure (Fig. 3C). With the ripening going on (> 5 h), MCM shows an irregular morphology (Fig. 3D). This is attributed to the formation of overlarge O_1 core in W phase (Fig. 2F), resulting in the formation of overlarge pores, which easily collapse under capillary force during the dying and form the irregular aggregation. Given the formation mechanism, the macropore size can be tuned according to the demand in applications by changing the ripening time,. Based on the requirements of protein separation and purification, we chose MCM solidified at the early stage (1 h) as the chromatographic media due to its relatively homogeneous macroporous structure.

The external morphology of MCM was observed by an optical microscope (Fig. 3E). The microsphere diameter of MCM is about ranging from 60 to 100 μm (Fig. S4). It can be seen from Fig. 3E that there is large void inside MCM, which results from the coalescence between O_1 as above-mentioned. The meso/micropore of MCM was investigated by N_2 adsorption/desorption isotherm measurements (Fig. 3F). MCM has a typical IV-type adsorption/desorption isotherm with obvious H4 hysteric loops, indicating the presence of mesopores, as demonstrated by the pore size distributions (Fig. 3E). The porosity and specific surface area of MCM are 92.62% and 169.84 m^2/g, respectively. The high porosity and specific surface area are beneficial for high adsorption capacity. MCM was further modified with DEAE-HCl to fabricate an ion-exchange adsorbent (DEAE-MCM) for protein separation.

The successful modification of DEAE groups onto MCM was confirmed by FT-IR and XPS spectra, as shown in Fig. 4A, B. Compared with raw cellulose and MCM, DEAE-MCM shows a new absorption peak at 1316 cm^{-1}, which is assigned to the stretching vibration of C-N originating from DEAE groups. Moreover, the intensity of the O–H stretching vibration of DEAE-MCM at 3300–3600 cm^{-1} is lower than that of raw cellulose and MCM, which is due to that the grafting of DEAE groups consumes partial O–H groups. In the XPS spectra (Fig. 4B), a

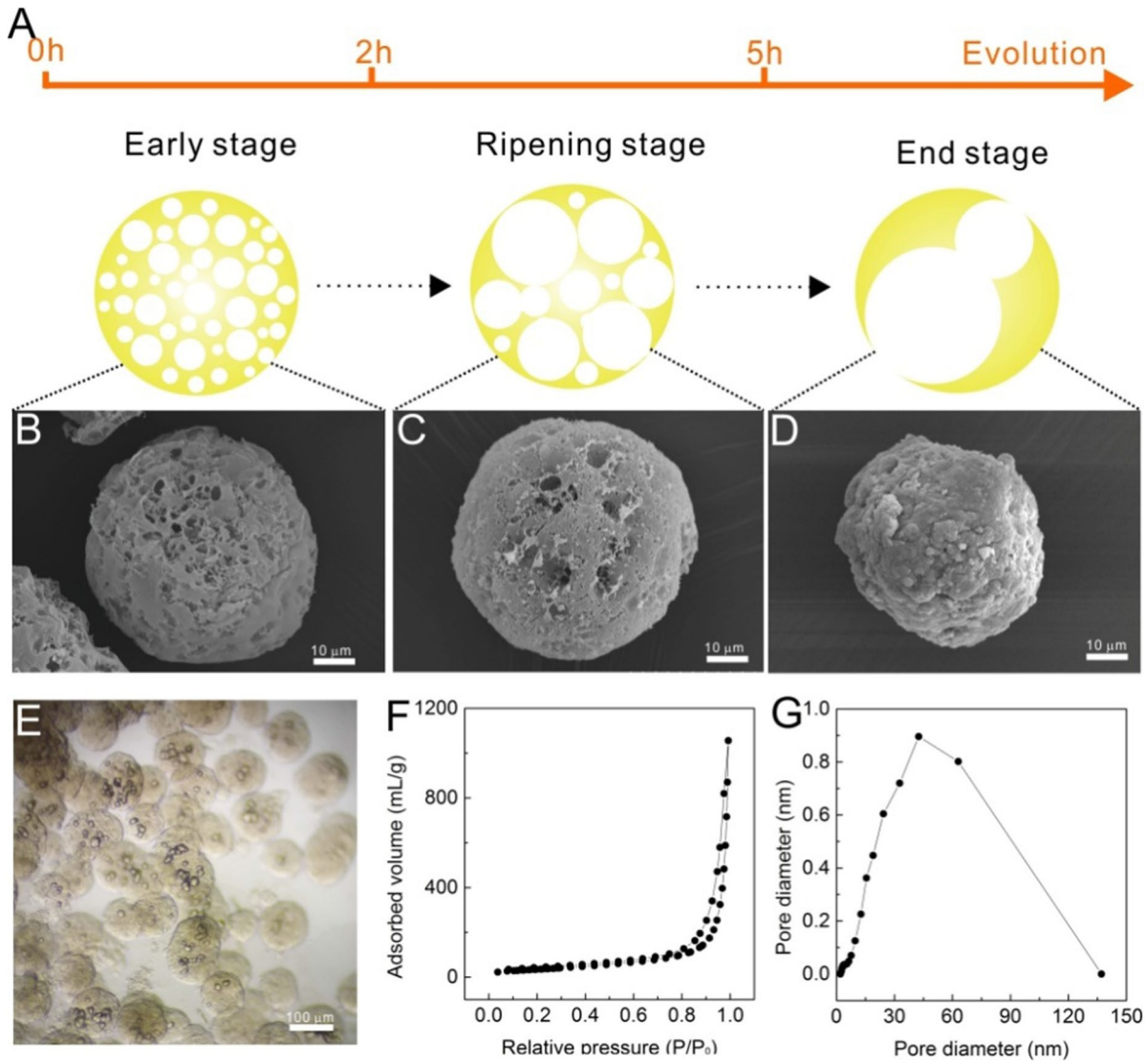

Fig. 3 Morphology evolution (**A**) of MCM with the increase of emulsion time and the corresponding SEM image (**B**–**D**). Optical micrograph (**E**), N_2 adsorption/desorption isotherms (**F**), and pore size distributions (**G**) of MCM

pronounced peak representing N atoms appears at 399.9 eV in the spectra of DEAE-MCM. The ionic capacity of DEAE-MCM measured by silver chloride precipitation titration reaches 304.23 mmol/g, which is much higher than that of commercial and previously reported chromatographic media (Bai et al. 2018; Lu et al. 2012). Figure 4C shows XRD patterns of raw cellulose, MCM, and DEAE-MCM. The raw cellulose shows four peaks at 14.8°, 16.3°, 22.7°, and 34.3°, which are assigned to cellulose I crystal. MCM shows three peaks at = 12.2, 20.2, and 21.9°, which are assigned to the $(1\bar{1}0)$, (110), and (020) planes of the cellulose II crystal. DEAE-MCM shows a similar XRD pattern to MCM, indicating that the modification has no effect on the cellulose crystal.

The microstructure of DEAE-MCM was observed and compared with commercial DEAE-FF by optical microscope and SEM, as shown in Fig. 5. DEAE-MCM and DEAE-FF have a similar microsphere diameter of about 60–120 μm (Fig. 5A, E, S5, and S6). Noted that there is a great difference in optical property between DEAE-MCM and DEAE-FF.

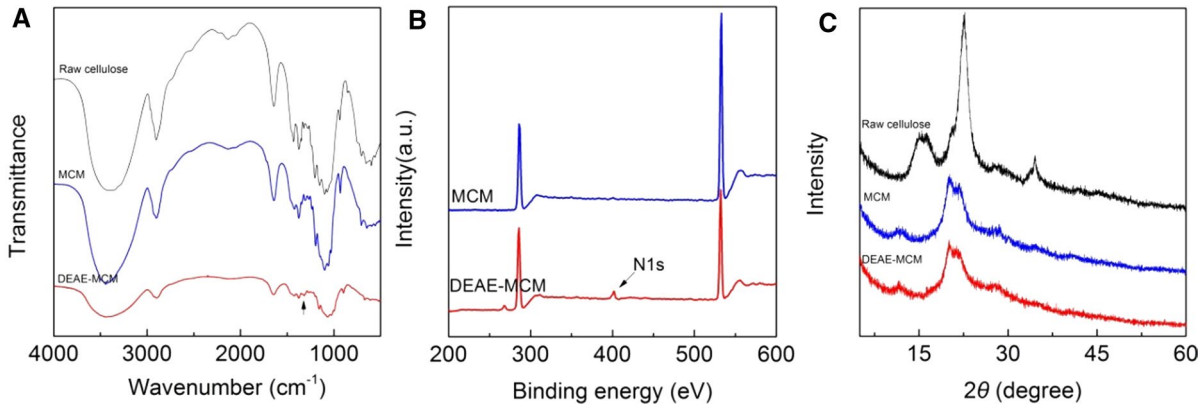

Fig. 4 FT-IR spectra (**A**), XPS (**B**), and XRD patterns (**C**) of raw cellulose, MCM, and DEAE-MCM

DEAE-MCM has an obvious light scattering, while DEAE-FF exhibits homogeneous optical phenomena (Fig. 5A, E), indicating that there is a significant difference in the intraparticle structure, evidenced by the following SEM images (Fig. 5B–D, F–H). DEAE-MCM remains its initial macroporous structure with an average pore diameter of 1.34 μm (Fig. S7), while DEAE-FF shows a relatively smooth and compact surface without visible macroporous structure. The macroporous structure is favorable to provide unimpeded mass-transfer paths for proteins, increasing the permeability and improving adsorption kinetic. Moreover, swelling experiments (Fig. S8) reveal that DEAE-MCM has no obvious volume change at different buffer solutions, indicating the solution stability.

Pore properties of DEAE-MCM

To verify the improvement of the macroporous structure on the mass transfer, we investigated the effect of flow rate on the back pressure and bed permeability of DEAE-MCM and DEAE-FF packed columns. As shown in Fig. 6A, the back pressure of both DEAE-MCM and DEAE-FF column increases linearly with the increasing flow rate ranging from 0 to 4.5 mL/min cm^2, indicating both microspheres are mechanical stable during operations. Importantly, it is noticed that the back pressure of DEAE-MCM is much lower than that of DEAE-FF under the same flow rate of mobile phase. The gap remains stable at the flow rate of 0 to 4.5 mL/min cm^2. The lower back pressure of DEAE-MCM is attributed to the presence of the macroporous structure, which causes the convective flow in the intraparticle structure and improves mass transfer rate (Zhai et al. 2012). Based on the experimental data, the bed permeability (K) was calculated according to the Darcy's model as follows (Rodrigues et al. 1995):

$$K = \frac{\mu u L}{\Delta P} \tag{7}$$

where μ (Pa s) is the viscosity of the mobile phase; u (m/s) is the superficial velocity of the mobile phase; L (m) is the length of the column; ΔP (Pa) is the pressure drop of the column. The bed permeability of DEAE-MCM reaches 3.81×10^{-13} m^2, much higher than that of DEAE-FF column (2.29×10^{-13} m^2) (Fig. 6B). The low pressure and high permeability of DEAE-MCM make it suitable as a promising chromatographic media for fast protein separation.

The meso/microporous structure of DEAE-MCM and DEAE-FF was investigated by N_2 adsorption/desorption isotherm measurements, as shown in Fig. 7A. Both microspheres are typical IV-type adsorption/desorption isotherms with obvious H4 hysteric loops, indicating the presence of mesopores, as demonstrated by the pore size distributions. The pore size mainly distributes between 10 and 100 nm in Fig. 7B. One should be noticed that, although the introduction of macropores in DEAE-MCM, which usually consumes many meso/micropores, the mesopore volume of DEAE-MCM (1.63 mL/g) is still much higher than that of DEAE-FF (0.20 mL/g). The specific surface area (SSA) of DEAE-MCM (171.31 m^2/g) also has no obvious change, higher than that of DEAE-FF (36.90 m^2/g).

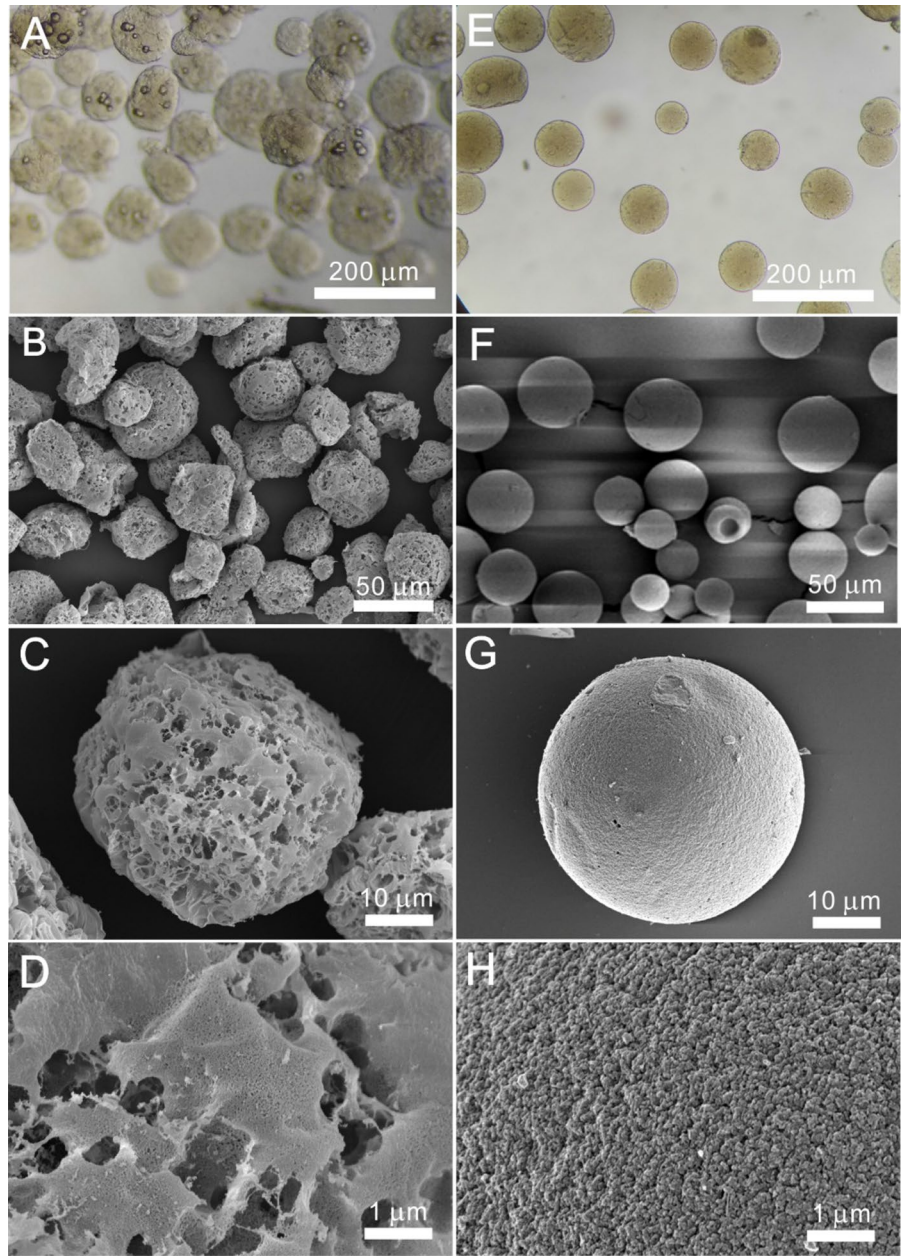

Fig. 5 Optical micrographs and SEM images of DEAE-MCM (**A**–**D**) and DEAE-FF (**E**–**H**)

This means that DEAE-MCM not only can provide wide transfer channels for protein diffusing but also has abundant adsorption sites for high adsorption capacity. The high SSA is probably associated with the recrystallization of NaOH and thiourea during the solidification by ethanol, which serves as a mesopore porogen embedded between cellulose nanofibers. Moreover, fractal dimension (D) was calculated to analyze the porous structure according to Frenkel–Halsey–Hill (FHH) model (Sahouli et al. 1997) (Fig. 7C). The D values of DEAE-MCM and DEAE-FF are 2.22 and 2.14, respectively, indicating DEAE-MCM has a more tortuous porous structure. Such tortuous porous structure can provide substantial interconnected porous channels, significantly improving the mass transfer rate of proteins.

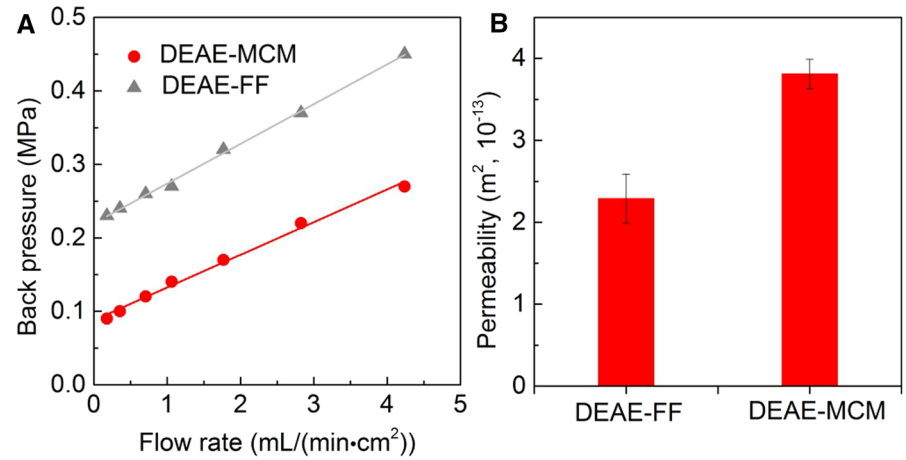

Fig. 6 Flow hydrodynamics curves (**A**) and permeability (**B**) of DEAE-MCM and DEAE-FF (Water as mobile phase)

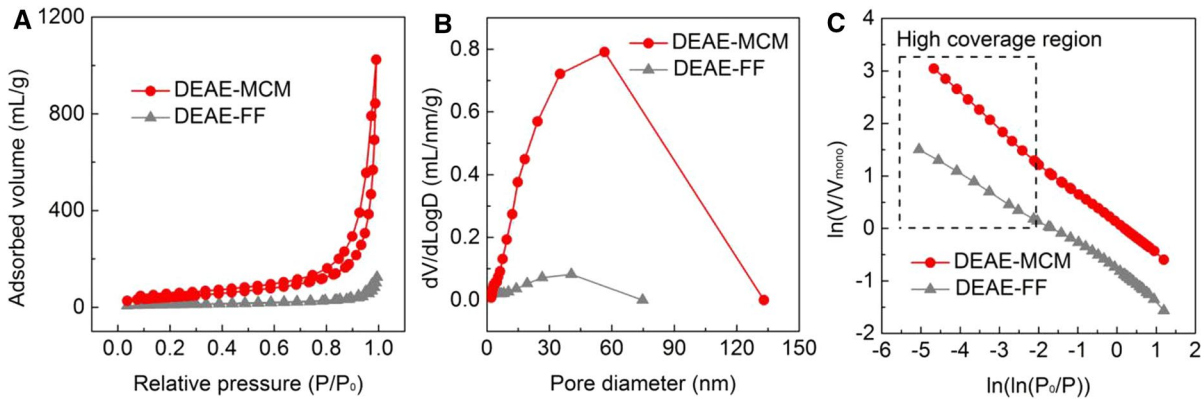

Fig. 7 N_2 adsorption/desorption isotherms (**A**), pore size distributions (**B**), and FHH plots from the N_2 adsorption/desorption isotherms (**C**) of DEAE-MCM and DEAE-FF

Protein adsorption evaluation

The combination of macropores and high SSA of DEAE-MCM makes it a promising adsorbent for proteins. Kinetic and isothermal BSA adsorption processes were systemically investigated. Figure 8A shows the effect of adsorption time on the adsorption amount of BSA. MCM, DEAE-MCM, and DEAE-FF exhibit similar adsorption behaviors. Initially, the adsorption amounts increase with the increase of adsorption time and then reach equilibrium. The adsorption data were fitted by pseudo-first-order and pseudo-second-order kinetic models, respectively. Pseudo-first-order model shows a higher correlation coefficient (R^2) (Table S1). The adsorption kinetic of MCM was not fitted due to the poor fitting between the data and kinetic models. According to the model, DEAE-MCM has a high adsorption amount of 326.12 mg/g within 40 min, far superior to unmodified MCM with 17.80 mg/g and commercial DEAE-FF with 59.79 mg/g. The fast adsorption kinetic is attributed to the macroporous structure of DEAE-MCM, which allows the convective flow of BSA in the inner structure of the microspheres, decreasing the mass transfer resistance and improving the adsorption rate. Fast adsorption kinetic is essential for protein separation and purification, which can decrease the cost and improve process efficiency.

Moreover, DEAE-MCM also has a higher BSA adsorption capacity compared with DEAE-FF. As shown in Fig. 8B, the maximum adsorption capacity of DEAE-MCM reaches 334.21 mg/g, which

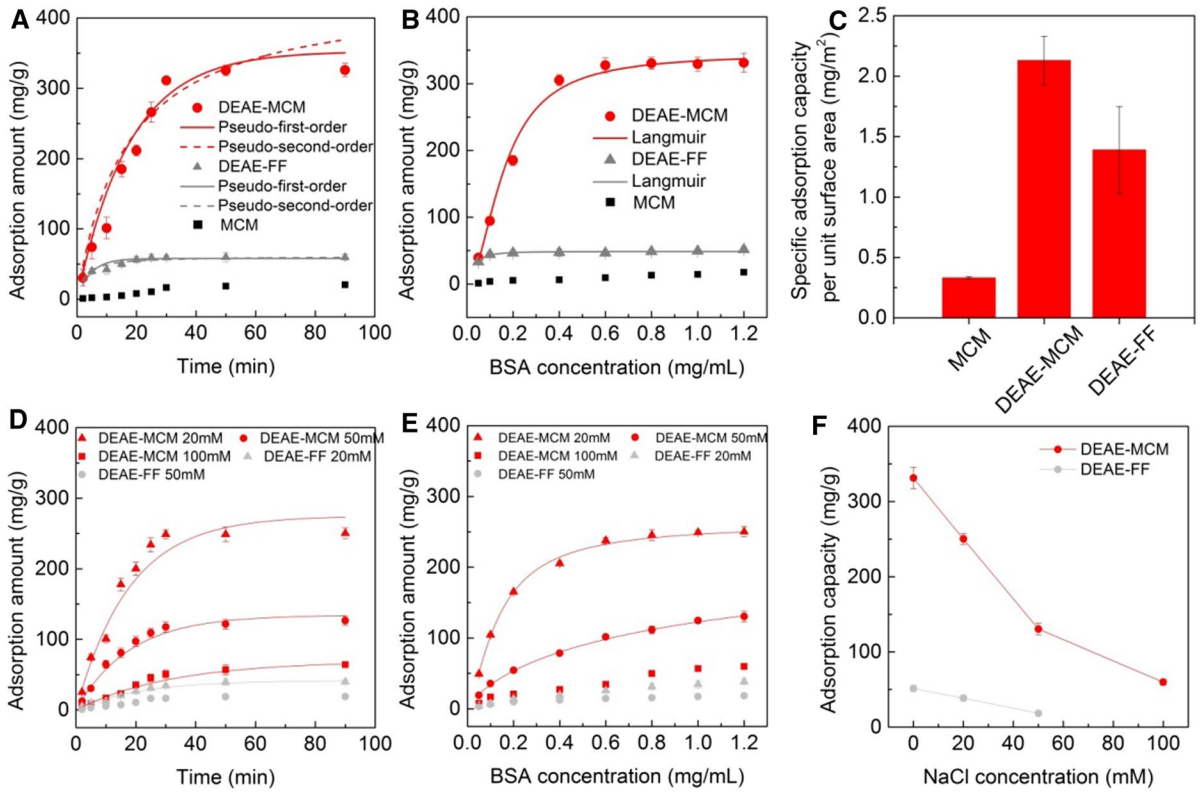

Fig. 8 Adsorption kinetics (**A**), adsorption isotherms (**B**), and specific adsorption capacity per unit surface area (**C**) of BSA of DEAE-MCM, DEAE-FF, and MCM; ionic strength effect on the adsorption kinetics (**D**) and isotherms (**E**) of DEAE-MCM and DEAE-FF; adsorption capacities (**F**) of DEAE-MCM and DEAE-FF at different ionic strength

is over 16 times and 5.4 times higher than that of MCM (20.10 mg/g) and DEAE-FF (59.89 mg/g), respectively. Such high adsorption capacity of DEAE-MCM also surpasses that of most reported cellulose-based adsorbents (Du et al. 2010; Lan et al. 2015; Qiao et al. 2020) (Table S2). The high adsorption capacity is associated with its high SSA, which provides abundant adsorption sites for BSA. The adsorption isotherm was fitted with Langmuir model, yielding high coefficients (R^2) of 0.99 and 0.97 for DEAE-MCM and DEAE-FF, respectively. Notably that the high adsorption capacity of DEAE-MCM did not only depend on its high specific surface area. As shown in Fig. 8C, the specific adsorption capacity per unit surface area of DEAE-MCM reaches 2.13 mg/m^2, which is higher than that of DEAE-FF (1.39 mg/m^2). The phenomenon indicates that the adsorption sites of DEAE-MCM are easier to contact with BSA than that of DEAE-FF, which is attributed to the macroporous structure as a reservoir improves the meso/micropore accessibility and utilization and enables more ligands on the inner surface of microspheres to sufficiently contact with BSA.

Ionic strength has an important impact on protein adsorption and elution behaviors. Generally, proteins are bound at low ionic strength and eluted at high ionic strength. Figure 8D–F show the adsorption isotherms and kinetics of DEAE-MCM and DEAE-FF at different salt concentrations. With the increase of salt concentration from 20 to 100 mM, the adsorption capacities of DEAE-MCM and DEAE-FF decrease from 250.26 mg to 59.80 mg/g and from 38.60 to 0.00 mg/g (Fig. 8D–F), respectively. The decreasing adsorption capacities are due to the screening of the electrostatic interactions between proteins and ligands at high ionic strength. Accordingly, the adsorption rates of DEAE-MCM and DEAE-FF decrease with the increase of salt concentration. Despite this, the adsorption capacity and kinetic of DEAE-MCM

are superior to these of DEAE-FF at the same salt concentration.

The reusability of the adsorbent is also important for reducing the overall costs. The saturated BSA-adsorbed DEAE-MCM was immersed into 1.0 mol/L of NaCl solution to conduct desorption. After five consecutive adsorption/desorption cycles, the adsorption capacity of DEAE-MCM shows an obvious decrease from 326.12 mg/g to 250.36 mg/g (Fig. 9A). The decrease is due to the fragmentation and collapse of macroporous structure, as demonstrated in Fig. 9B. The macroporous structure caused its poor mechanical strength. This also is a long-standing challenge in chromatographic media having both macroporous structure and high mechanical strength because these properties are in general mutually exclusive. We will further improve our preparation technique to increase the mechanical strength of DEAE-MCM in future study. BSA concentration in the eluent was determined at 280 nm. The recovery of BSA on DEAE-MCM was estimated to be 84.5 ± 4.3%, which is comparable with most reported resins (Li et al. 2017; Xu et al. 2020), indicating the stability of DEAE-MCM and high yield of protein elution.

To further explore the potential use of DEAE-MCM, breakthrough experiments were carried out to investigate the effect of the flow rate of mobile phase on the dynamic adsorption capacity (DBC). The DBC was calculated according to the breakthrough curves at the breakthrough point of 10% (Fig. 10A). At the flow rate of 0.88 mL/min cm^2, the DBC of DEAE-MCM reaches about 250 mg/g, far exceeding that of DEAE-FF (about 45 mg/g). More important, the DBC/q_m value (the ratio of DBC to static maximum adsorption capacity) of DEAE-MCM remains relatively stable (Fig. 10B). In contrast, the DBC/q_m value of DEAE-FF presents a drastic decrease. The result indicates that DEAE-MCM retains its high

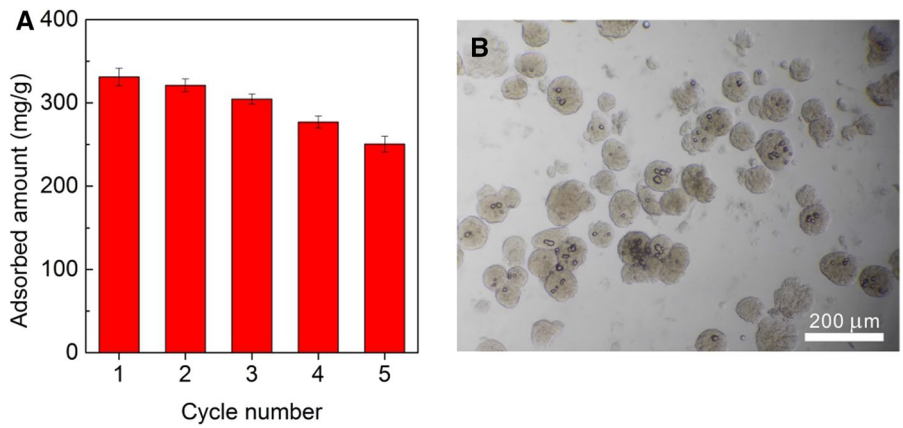

Fig. 9 Reusability of DEAE-MCM (**A**) and its optical micrograph (**B**) after five consecutive adsorption/desorption cycles

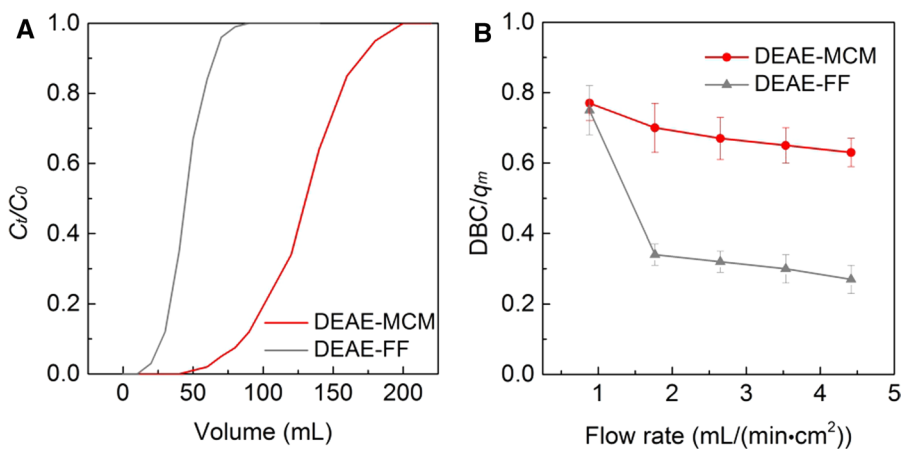

Fig. 10 BSA Breakthrough curves of DEAE-MCM and DEAE-FF (**A**); effect of flow rate on the DBC/q_m (**B**)

adsorption capacity even at high operation flow rate, promising for use in fast protein chromatography.

Conclusion

In summary, macroporous cellulose microspheres (MCM) with enhanced mass transfer ability were successfully fabricated by a double emulsion method. The macroporous structure not only provided wide channels for mass transfer but also increased the accessibility and utilization of meso/micropores. Further, the obtained MCM was modified by DEAE to achieve an anion-exchange adsorbent (DEAE-MCM). Befitting from the advantages of the macroporous structure, the obtained DEAE-MCM showed not only a high permeability (3.81×10^{-13} m^2), but also fast adsorption kinetic (reaching equilibrium within 40 min) and high adsorption capacity of 334.21 mg/g for BSA, which were significantly superior to commercial DEAE-FF. More importantly, DEAE-MCM remained a high dynamic adsorption capacity even at a high operation flow rate in breakthrough experiments, promising for use in fast protein chromatography. Moreover, we believe that MCM also offers excellent prospects in applications that benefit from its properties, such as tissue engineering and drug delivery.

Acknowledgments The work was funded by Natural Science Foundation of China (21676170). We also thank Yanping Huang from Center of Engineering Experimental Teaching, School of Chemical Engineering, Sichuan University for the help of SEM image.

Funding The authors have not disclosed any funding.

Declarations

Conflict of interest The authors declare no conflict of interests.

References

Bai S, Gong LL, Han DT, Li YT, Yu LL, Sun Y (2018) Protein adsorption onto diethylaminoethyl dextran modified anion exchanger: effect of ionic strength and column behavior. Chin J Chem Eng 26:259–267

Beyki MH, Mohammadirad M, Shemirani F, Saboury AA (2017) Magnetic cellulose ionomer/layered double hydroxide: an efficient anion exchange platform with enhanced diclofenac adsorption property. Carbohydr Polym 157:438–446

Bowes BD, Lenhoff AM (2011) Protein adsorption and transport in dextran-modified ion-exchange media. II. Intraparticle uptake and column breakthrough. J Chromatogr A 1218:4698–4708

Du KF, Yan M, Wang QY, Song H (2010) Preparation and characterization of novel macroporous cellulose beads regenerated from ionic liquid for fast chromatography. J Chromatogr A 1217:1298–1304

Farid SS, Baron M, Stamatis C, Nie WH, Coffman J (2020) Benchmarking biopharmaceutical process development and manufacturing cost contributions to R&D. Mabs-Austin 12:1754999

Feng CT, Ren PG, Huo MX, Dai Z, Liang D, Jin YL, Ren F (2020) Facile synthesis of trimethylammonium grafted cellulose foams with high capacity for selective adsorption of anionic dyes from water. Carbohydr Polym 241:116369

Fu QX, Wang XQ, Si Y, Liu LF, Yu JY, Ding B (2016) Scalable fabrication of electrospun nanofibrous membranes functionalized with citric acid for high-performance protein adsorption. ACS Appl Mater Interfaces 8:11819–11829

Gao F, Su ZG, Wang P, Ma GH (2009) Double emulsion templated microcapsules with single hollow cavities and thickness-controllable shells. Langmuir 25:3832–3838. https://doi.org/10.1021/la804173b

Gericke M, Trygg J, Fardim P (2013) Functional cellulose beads: preparation, characterization, and applications. Chem Rev 113:4812–4836

Gustavsson PE, Larsson PO (1999) Continuous superporous agarose beds for chromatography and electrophoresis. J Chromatogr A 832:29–39

Lan T, Shao ZQ, Wang JQ, Gu MJ (2015) Fabrication of hydroxyapatite nanoparticles decorated cellulose triacetate nanofibers for protein adsorption by coaxial electrospinning. Chem Eng J 260:818–825

Li XQ, Li Q, Gong FL, Lei JD, Zhao X, Ma GH, Su ZG (2015) Preparation of large-sized highly uniform agarose beads by novel rotating membrane emulsification. J Membr Sci 476:30–39

Li XX, Liu Y, Sun Y (2017) Alginate-grafted Sepharose FF: A novel polymeric ligand-based cation exchanger for high-capacity protein chromatography. Biochem Eng J 126:50–57

Love JC, Love KR, Barone PW (2013) Enabling global access to high-quality biopharmaceuticals. Curr Opin Chem Eng 2:383–390

Lu HL, Lin DQ, Zhu MM, Yao SJ (2012) Protein adsorption on DEAE ion-exchange resins with different ligand densities and pore sizes. J Sep Sci 35:3084–3090

Na XM, Gao F, Zhang LY, Su ZG, Ma GH (2012) Biodegradable microcapsules prepared by self-Healing of porous microspheres. ACS Macro Lett 1:697–700

Oshima T, Taguchi S, Ohe K, Baba Y (2011) Phosphorylated bacterial cellulose for adsorption of proteins. Carbohydr Polym 83:953–958

Oshima T, Sakamoto T, Ohe K, Baba Y (2014) Cellulose aerogel regenerated from ionic liquid solution for immobilized metal affinity adsorption. Carbohydr Polym 103:62–69

Qiao LZ, Zhao LS, Ai H, Li YL, Liu Y, Du KF (2019) Diethylaminoethyl-modified magnetic starlike organic spherical

adsorbent: fabrication, characterization, and potential for protein adsorption. Ind Eng Chem Res 58:4099–4107
Qiao LZ, Li SS, Du KF (2020) Fabrication and characterization of porous cellulose beads with high strength and specific surface area via preliminary chemical cross-linking reaction for protein separation. Biochem Eng J 153:107412
Rodrigues AE, Loureiro JM, Chenou C, Delavega MR (1995) Bioseparations with permeable particles. J Chromatogr B 664:233–240
Roy D, Semsarilar M, Guthrie JT, Perrier S (2009) Cellulose modification by polymer grafting: a review. Chem Soc Rev 38:2046–2064
Sahouli B, Blacher S, Brouers F (1997) Applicability of the fractal FHH equation. Langmuir 13:4391–4394
Schlitz HK (1984) Protein purification: principles and practice—Scopes, R. Biochem Educ 12:143. https://doi.org/10.1016/0307-4412(84)90112-2
Sehaqui H, Salajkova M, Zhou Q, Berglund LA (2010) Mechanical performance tailoring of tough ultra-high porosity foams prepared from cellulose I nanofiber suspensions. Soft Matter 6:1824–1832
Shukla AA, Hubbard B, Tressel T, Guhan S, Low D (2007) Downstream processing of monoclonal antibodies—application of platform approaches. J Chromatogr B 848:28–39
Smith C (2005) Striving for purity: advances in protein purification. Nat Methods 2:71–77
Song YY, Fan JB, Li XL, Liang XM, Wang ST (2019) pH-regulated heterostructure porous particles enable similarly sized protein separation. Adv Mater 31:1900391
Wang DM, Hao G, Shi QH, Sun Y (2007) Fabrication and characterization of superporous cellulose bead for high-speed protein chromatography. J Chromatogr A 1146:32–40
Xu R, Li XX, Dong XY, Sun Y (2020) Protein cation exchangers derived by charge reversal from poly(ethylenimine)-Sepharose FF: comparisons between two derivatization routes. J Chromatogr A 1611:460586
Yu LL, Sun Y (2013) Protein adsorption to poly(ethylenimine)-modified Sepharose FF: II. Effect of ionic strength. J Chromatogr A 1305:85–93
Zhai YQ, Zhou WQ, Wei W, Qu JB, Lei JD, Su ZG, Ma GH (2012) Functional gigaporous polystyrene microspheres facilitating separation of poly(ethylene glycol)-protein conjugate. Anal Chim Acta 712:152–161
Zhang RY et al (2014) Hydrophilic modification gigaporous resins with poly(ethylenimine) for high-throughput proteins ion-exchange chromatography. J Chromatogr A 1343:109–118
Zhao X et al (2019) Fabrication of rigid and macroporous agarose microspheres by pre-cross-linking and surfactant micelles swelling method. Colloid Surface B 182:110377